Detailed Structure of Molecularly Thin Polyelectrolyte Multilayer Films on Solid Substrates as Revealed by Neutron Reflectometry

Mathias Lösche,*,† Johannes Schmitt,‡ Gero Decher,‡,§ Wim G. Bouwman,∥,⊥ and Kristian Kjaer∥

Institute of Experimental Physics I, University of Leipzig, D-04103 Leipzig, Germany, Institute Charles Sadron, C.N.R.S., F-67083 Strasbourg, France, Université L. Pasteur, F-67083 Strasbourg, France, Physics Department, Risø National Laboratory, DK-4000 Roskilde, Denmark

Received June 9, 1998

ABSTRACT: Using neutron reflectometry we have resolved—to high resolution—the internal structure of self-assembled polyelectrolyte multilayer films and have developed a detailed molecular picture of such systems by analyzing the data with a composition-space refinement technique. We show that such surface films consist of stratified structures in which polyanions and polycations of individual layers interdigitate one another intimately. Nevertheless, the deposition technique leads to results that are predictable, if well-defined and constant environmental conditions are maintained during the preparation. For alternating layers of poly(styrenesulfonate) (PSS) and poly(allylamine hydrochloride) (PAH), adsorbed onto atomically flat surfaces, a roughening of successively deposited layers leads to a progressively larger number of adsorption sites for consecutive generations of adsorbed polymer, and thus to an increase in layer thicknesses with an increasing number of deposited layers. Because of the interpenetration of adjacent polyelectrolyte species, however, this increase settles quickly into an equilibrium thickness. In fully hydrated films (100% relative humidity), water occupies ≥40% of the volume within the films. About twice as much water (by volume) is associated with PSS as with PAH. Incorporated inorganic salt plays a minor role only, if any. The equilibrium thickness of the deposited layer structure may be fine-tuned via the ionic strength, I, of the solutions used for the preparation. We show that the dependence of the thickness d_{lp} per layer pair on I is linear, with a sensitivity, $\Delta d_{lp}/\Delta I = 16$ Å × L/mol. Concurrently with the layer thickness the interface roughness σ between adjacent layers increases: $\sigma \sim 0.4 \times d_{lp}$. In contrast to the ionic strength of the deposition solutions, the degree of polymerization of the polyanions used in the preparation plays a minor role only in determining the overall structure of the deposited films. The results reported here are quantitatively consistent with those of a recent study (Tarabia et al. *J. Appl. Phys.* **1998**, *83*, 725−732), if one assumes that the hydration of the polyelectrolyte molecules in the sample films investigated in the two studies is similar.

Introduction

Thin polymer films are widely used for the modification and functionalization of surfaces. The adsorption from solutions of molecularly organized polyelectrolyte multilayer films is a particularly refined technology for modifying surfaces for advanced applications. It has been well documented that the physisorption or chemisorption of polyelectrolytes or reactive polymers onto surface-functionalized substrates can lead to the deposition of molecularly thin surface films.[1] It has been further established that a great variety of technologically important uncharged substrates can be prepared for the deposition of various polyelectrolytes by covalent bonding of chargeable species, e.g., amino-functionalized silanes or thiols. Arbitrarily shaped surfaces can be modified as long as they are accessible to the solvent. Upon sequential dipping of the substrates into solutions of alternately charged polyelectrolytes, this deposition is iterated, resulting in the formation of progressively thicker polymer films. Semiquantitatively, UV absorption and small-angle X-ray reflection (SAXR) measurements have shown that the adsorption of alternately charged film increments occurs linearly with the number of dipping cycles once a few layers have been deposited on the substrate.[2] The thickness of such layer increments depends on physicochemical conditions such as the salt content of the polyelectrolyte solutions.[3−5]

With this technique, ultrathin conducting layers can be applied to various materials,[6] providing a general route to invisible antistatic coatings, and the construction of molecularly thin organic photodiodes may be feasible.[4,6,7] Lateral patterning on the micrometer-length scale is feasible by lithography[8] or microcontact printing.[9] Because the deposition of polyelectrolytes generally occurs from aqueous solutions, the production process is environmentally safe, and, depending on the polyelectrolytes used, the surface films may be "biocompatible": proteins adsorbed or conjugated to such polymer interface films retain their functional integrity. This has been exploited for the immobilization of various biomolecules at modified surfaces and for the construction of molecularly well-organized biosensoric interface films.[10]

The attractiveness of molecular polyelectrolyte interface films derives both from the diversity of options that it provides for surface functionalization through chemical variation of the adsorbent molecules and from the possibility to control the molecular architecture of the surface film by the physicochemical conditions of its preparation.[1] Variation of the preparation parameters may also be exploited for mechanistic studies of the

† University of Leipzig.
‡ Institute Charles Sadron.
§ Université L. Pasteur.
∥ Risø National Laboratory.
⊥ Current address: Technical University of Delft, Interfacultair Reactor Institute, NL-2629 JB Delft, The Netherlands.

10.1021/ma980910p CCC: $15.00
Published on Web 11/26/1998

Table 1. Layer Sequence and Preparation Conditions of the Samples Investigated in This Study

sample	layer sequence in repeat unit (r.u.)	(*n*) r.u.'s	(*n*) layers[a]	[NaCl][b] (M)	degree of polymerization[c] PSS-h_7	PSS-d_7
A1	[PSS-h_7−PAH−PSS-d_7−PAH][d]	8	32	2	410	880
A2	[(PSS-h_7−PAH)$_2$−PSS-d_7−PAH][e]	8	48	2	410	880
A3	[PSS-d_7−PAH]	10	20	2	410	880
B3	[(PSS-h_7−PAH)$_3$−PSS-d_7−PAH]	8	64	2	900	880
B4	[(PSS-h_7−PAH)$_3$−PSS-d_7−PAH]	8	64	2	5250	4800
B5	[(PSS-h_7−PAH)$_4$−PSS-d_7−PAH]	8	80	0.5	900	880
B6	[(PSS-h_7−PAH)$_4$−PSS-d_7−PAH]	8	80	0.5	5250	4800
B7	[(PSS-h_7−PAH)$_4$−PSS-d_7−PAH]	8	80	1	900	880
B8	[(PSS-h_7−PAH)$_3$−PSS-d_7−PAH]	8	64	3	900	880

[a] Total number of polyelectrolyte layers without first ABS layer. [b] NaCl concentration of PSS and PAH solutions used for sample preparation. [c] Degree of polymerization of PAH used in all preparations: 530−700. [d] Sample B and [e]sample C of ref 11.

adsorption process. Such a systematic investigation of the structural properties of surface films under different preparation conditions is the aim of the work reported here.

In previous work, we showed that neutron reflection is a particularly powerful method for the structural characterization of surface films that incorporate protonated and deuterated polyelectrolytes.[11] We demonstrated that the preparation technique yields stable, molecularly stratified film structures, as suggested from the mode of preparation. The internal structure of the surface films in terms of their polymer density, water content, and interdigitation of the polymer segments between adjacent layers was assessed. Similarly, a recent study focused on combined neutron and X-ray reflectivity measurements on stratified samples that included a conjugated polymer, poly(phenylenevinylene) (PPV), in the film structure.[12] In this report, we extended our earlier work into a systematic structural characterization of surface films deposited from different salt concentrations and different molecular weights of the polyelectrolytes. Compared with earlier work we now considerably improved the resolution of the measurements enabling a characterization of structural defects along the surface normal.

Experimental Section

Sample Preparation. Polyelectrolyte multilayer samples with protonated/deuterated layer sequences were prepared as described previously.[11] Silicon substrates (∼ 45 × 140 × 0.7 mm) were cut from 6-in. wafers (Wacker, Burghausen, Germany). Poly(styrenesulfonate) sodium salt (PSS-h_7), M_w = 84,000, 184,000, and 1,070,000 (M_w/M_n < 1.1), were obtained from Polymer Standards (Mainz, Germany). Perdeuterated poly(styrenesulfonic acid) (PSS-d_7), M_w = 168,000 and M_w = 913,000 (M_w/M_n < 1.1) were prepared as described.[11] Poly(allylamine) hydrochloride (PAH), M_w = 50,000−65,000 was from Aldrich (Steinheim, Germany). 4-Aminobutyldimethylmethoxysilane (ABS) was from ABCR (Karlsruhe, Germany). Water was prepurified by reverse osmosis and filtered (Milli-Q, Millipore GmbH, Eschborn, Germany) to obtain a resistance $\rho \geq 18$ MΩcm. All solvents were of p.a. grade (Merck, Darmstadt, Germany).

Si substrates were cleaned in $H_2O/H_2O_2/NH_3$ (5:1:1 v/v/v) at T = 80 °C for ∼15 min, followed by extensive rinsing with water. To obtain a homogeneously distributed surface charge, freshly cleaned Si substrates were precoated with an ABS film as described,[11] after washing with methanol, methanol/toluene (1:1 v/v), and toluene. After deposition of the ABS, the wafers were washed again in toluene, methanol/toluene (1:1), and methanol. After the deposition of a first charged molecular layer, an alternating series of polyanionic and polycationic layers was deposited by dipping the substrates for 20 min into aqueous solutions of protonated or deuterated PSS (3 mM PSS, 3 mM HCl, various concentrations of NaCl), washing for 3 × 1 min in H_2O, dipping for 20 min into an aqueous solution of PAH (3 mM PAH, 3 mM HCl, various concentrations of NaCl), and washing again for 3 × 1 min in H_2O. After the last wash, the sample was dried in either a N_2 gas stream or a stream of pressurized, filtered air. The PSS/PAH dipping cycle was repeated until the desired layer sequence had been completed. Samples of series A (see below) were hand-dipped, whereas samples of series B were prepared using a home-built, computer-controlled automated dipper.

As in earlier neutron reflectometry work, we prepared, on Si substrates, samples that incorporated, along the surface normal, $\hat{z}$, one-dimensional superlattices of protonated multilayers alternating with single deuterated layers. In this work, we measured the neutron reflectivity of samples prepared from PSS and PAH solutions with various NaCl concentrations and different molecular weights of the PSS; after preparation in H_2O-based solution, we dehydrated one of the samples over P_2O_5 and rehydrated it in D_2O. Table 1 gives a synopsis of the samples that we have characterized using neutron reflectometry.

Neutron Reflectometry and Data Analysis. Measurements were performed in the neutron guide hall of the DR3 reactor at Risø National Laboratory, either at the TAS7[13,14] reflectometer (now superseded by the Mark II reflectometer at port TAS9) with a vertical scattering plane (sample series A) or at the reflectometer at port TAS8,[15] which has a conventional geometry with a horizontal scattering plane (sample series B). The background in the measurements was determined experimentally for each data point[14] and subtracted. The wavelength was λ = 4.64 Å (TAS7 measurements) and λ = 4.74 Å (TAS8 measurements) and the momentum transfer $Q_z = 4\pi/\lambda \sin \theta_i$ was varied by scanning the grazing angle $\theta_i = \theta_f$. The resolution of the measurements was varied in discrete steps by changing the entrance and exit slit widths at several scattering angles, and the count times were adjusted for each data point such that the count statistics were approximately constant over the momentum transfer range investigated. Typical full widths at half-maximum of the momentum transfer resolution were between $\Delta Q_z = 10^{-3}$ and 5×10^{-3} Å^{-1} for TAS7 measurements and between $\Delta Q_z = 1.5 \times 10^{-4}$ and 1.5×10^{-3} Å^{-1} for TAS8 measurements.[16] All measurements were performed at room temperature. TAS8 measurements were conducted with the sample incorporated into an environmental chamber in which the humidity was adjusted to 100% relative humidity (r.h.) over a reservoir of H_2O or D_2O. TAS7 measurements were taken in ambient air.

Reflectivity data were analyzed to different levels of sophistication. We have shown[11] that a satisfactory description of the experimental data can be obtained with layer models, assuming that the adsorption of polyelectrolytes leads to a formation of n molecularly thin distinct strata that partially interpenetrate one another. This model is of the general form

$$\rho(z) = \sum_{i=0}^{n} \frac{\rho_{i+1} - \rho_i}{2} \times \left(1 - \mathrm{Erf}\left(\frac{z - z_i}{\sqrt{2}\sigma_i}\right)\right) \qquad (1)$$

where ρ denotes either the electron density, ρ_e, in X-ray

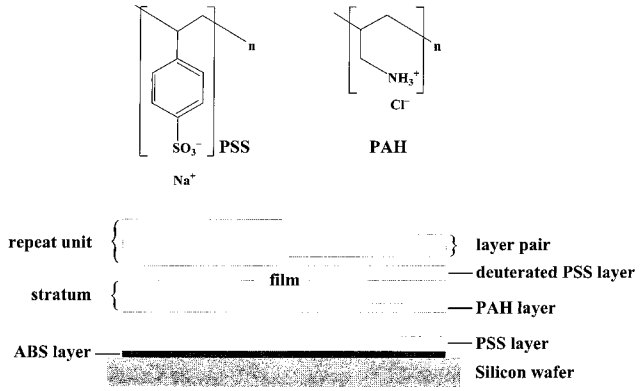

Figure 1. Structure of PSS and PAH and terms used to describe the layer system.

reflection or the neutron scattering length density (SLD), ρ_n, in neutron reflection measurements, and σ is the root-mean-square interfacial roughness.[17] Thus the profile consists of a sum of $n + 1$ step functions, smeared into error functions Erf(z), that are located at positions where the layers interpenetrate. Erf[$(z - z_0)/\sqrt{2}\sigma_{Si}$] describes the surface roughness of the Si substrate and Erf[$(z - z_n)/\sqrt{2}\sigma_{f/a}$] describes the surface roughness of the polymer film toward the ambient air. Because we recognized earlier[11] that a discrimination of adjacent protonated PSS and PAH layers cannot be afforded by the experimental data because of a lack of contrast,[18] we marked the individual strata with either a deuterated layer or several adjacent protonated (polycationic and polyanionic) layers. A wealth of structural information was gained from such a description in our earlier work.[11] However, two difficulties remained unresolved. (a) Because of a lack of Q_z resolution of the reflectometric experiment, all protonated/deuterated layer pairs had to be assumed identical in the evaluation, although it was clear that layers adsorbed closer to the substrate are thinner than layers further away from the substrate. (b) The interpenetration of polymer segments in adjacent layers leads to a coupling of the model parameters that describe layer thickness and scattering length density of the deuterated polyelectrolyte, seriously interfering with an unambiguous determination of the two quantities. As we will show, these problems are alleviated in this work by interpreting the scattering length densities in quasimolecular models.

Results

We investigated several polyelectrolyte multilayer samples, composed of PAH and protonated and deuterated PSS (see Figure 1), in which we systematically varied the salt concentration of the solution from which the films were deposited, the molecular weight of the polyanionic components, and the sequence of protonated and deuterated layers such that different one-dimensional repeat units within the stratified structures would result. We also investigated the water content of polyelectrolyte multilayer films and the rearrangement of the polymers upon dehydration.

To afford a clear distinction between layered structures of various hierarchical levels in the surface films, we will use the following terminology (cf. Figure 1): The term "layer" denotes an individual molecular polyanionic or polycationic layer as deposited from solution. We use this term independently of the fact that adjacent layers may interpenetrate each other substantially (i.e., σ_i in eq 1 may be of the same order as the layer thickness values d_i). The term "layer pair" is used for a polyanionic/polycationic twin. The term "stratum" denominates a succession of either deuterated or protonated layers, which is recognized as a layer sequence of (nearly) homogeneous scattering length density in the neutron reflectivity measurements (protonated strata may consist of 1, 3, 5 ... molecular layers, but deuterated strata consist of exactly 1 deuterated layer in all sample preparations discussed below). The "repeat unit" (r.u.) incorporates one deuterated layer plus several protonated layers (which may vary for different samples), i.e., it incorporates a protonated/deuterated pair of strata. Samples were constructed so that this layer sequence was repeated several times to form the complete surface structure, which is called a "film".

1. Variation of the Number of Layers in Protonated Strata. Figure 2 shows the neutron reflectivity of samples A2, A1, and A3 (top to bottom), measured over ~6 orders of magnitude. The films have been prepared from 2 M NaCl solutions using low molecular weight (LMW) polyelectrolytes (degree of polymerization, $P_w < 1000$) (see Table 1). The neutron reflectivities of samples A1 and A2, in which the spacing between the individual deuterated layers incorporates at least 3 protonated layers, show prominent Bragg reflections at $Q_z = 0.06$ Å^{-1} and at $Q_z = 0.04$ and 0.08 Å^{-1}, rising $\sim 1\,^1/_2$ decades over the Fresnel reflectivity. In contrast, no Bragg reflection is detected in the data from sample A3, in which deuterated layers are separated by just one (protonated) PAH layer.[19] The Kiessig fringes are more clearly developed in the reflectogram characterizing A3 than in those of A1 and A2, because of a larger average scattering length density and smaller overall thickness of the polymer film. As described earlier in detail,[11] the films have also been characterized in X-ray reflectivity measurements. These showed only Kiessig fringes but no Bragg peaks for any of the three samples (data not shown), because of a lack of contrast in ρ_e between adjacent polyelectrolyte layers.

The reflectivity data of sample A3 were analyzed more quantitatively in a simple model representing the polymer as a homogeneous surface film with different roughness values at its interfaces with the Si substrate and air. In all evaluations presented throughout this work, the substrate side of the interface layers was modeled with the same roughness $\sigma_{s/f} = \sigma_{Si} = 5$ Å, a value determined in X-ray reflectivity measurements of a blank. To describe the neutron reflectivity of A1 and A2, the samples were modeled as stratified surface films in which deuterated, PSS-d_7, layers were distinguished from protonated strata, incorporating PAH and PSS-h_7 layers (with no distinction between them).[11] Thus, both A1 and A2 were represented by 17 strata. In this model, 3 roughness values were discriminated: $\sigma_{s/f}$ between substrate and polymer film, $\sigma_{f/a}$ between polymer film and air, and σ_{int}, the interface roughness between adjacent deuterated and protonated strata. All scattering length densities of equivalent strata were assumed identical in samples A1 and A2. Similarly, thickness values were assumed to be identical except for the first protonated strata. The best-fit model parameters for the data shown in Figure 2 are summarized in Table 2, and the corresponding reflectivity models are included in Figure 2 as solid lines.

2. Variation of the Preparation Parameters. The higher resolution of the TAS8 instrument was used to characterize the structure of polyelectrolyte multilayer films in further detail. Figure 3a shows neutron reflectivity data of 4 films that have been adsorbed from polyelectrolyte solutions with different salt (NaCl) concentrations between 0.5 and 3 M as indicated. All films have been deposited using low molecular weight

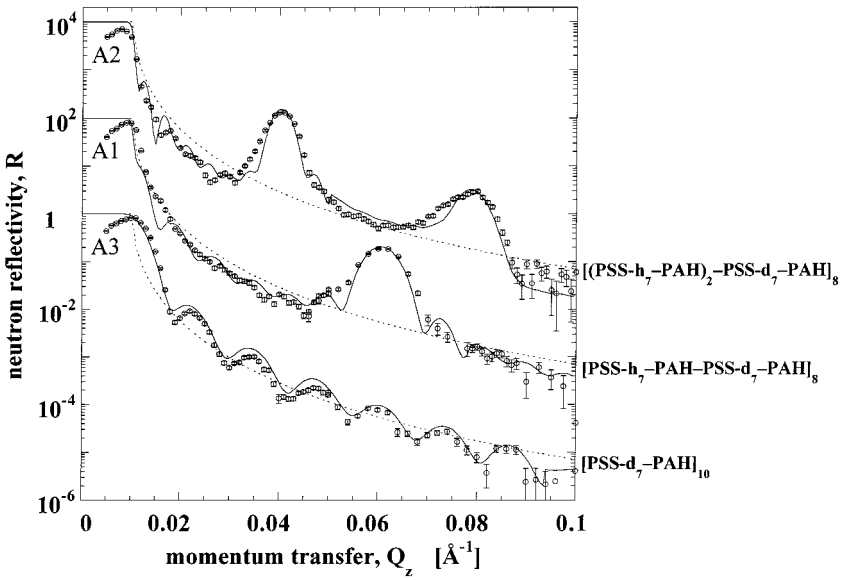

Figure 2. Neutron reflectivity of polyelectrolyte multilayer samples A2, A1, and A3 (top to bottom). In these samples, individual layers of PSS-d_7 are separated by 1 (A3), 3 (A1), and 5 (A2) fully protonated polyelectrolyte layers. The data points are supplemented with continuous lines representing the best-fit models as described in the text. The instrumental resolution has been included in the fits. Dotted lines indicate the Fresnel reflectivity of the Si substrate. For clarity, data sets A2 and A1 have been multiplied by 10^4 and 10^2, respectively. The data shown for A2 were also presented in ref 11.

Table 2. Structure of Films with 1 (Sample A3), 3 (A1), and 5 (A2) Protonated Molecular Polyelectrolyte Layers Deposited Between Deuterated Layers on Si Wafers[a]

sample	film thickness, d (Å) (X-ray)	film thickness, d (Å) (neutrons)	ρ_e (e^-/Å^3) of film	$\sigma_{f/a}$ (Å) (X-ray)	thickness of r.u. (Å)	SLD, ρ_n[10^{-6} Å^{-2}] protonated strata	SLD, ρ_n[10^{-6} Å^{-2}] deuterated strata	σ_{int} (Å) (neutrons)
A3	480 ± 5	475 ± 5	0.40	13 ± 1	–	2.90 ± 0.15		–
A1	785 ± 10	822 ± 15	0.41	15 ± 1	104.3 ± 2	0.87	3.1	20 ± 1
A2	1205 ± 20	1225 ± 15	0.409	14 ± 1	159 ± 2	0.87	3.1	19 ± 1

[a] ρ_e(Si) = 0.7 e^-/Å^3, ρ_n(Si) = 2.1 × 10^{-6} Å^{-2}, σ_{Si} = 5 Å. All polyelectrolyte films were deposited from LMW solutions with 2 M NaCl. Corresponding model reflectivities are shown as solid lines in Figure 1.

(LMW) compounds. Figure 3b compares, for two different ionic strengths, data for samples using LMW and high molecular weight (HMW) compounds.[20] The TAS8 data (Figure 3) show much more detail than the TAS7 data (Figure 2). Intricate patterns of well-developed Kiessig fringes are apparent in Figure 3, as well as several orders of Bragg peaks (some of which appear split, as discussed further below). First, we will discuss general aspects common to the reflectivity data sets from all samples before we proceed to evaluate the differences inferred by varying the salt concentration in the deposition solutions and by the molecular weight of the polyelectrolytes.

2a. General Structure of Deposited Films and Hydration: To assess the content and organization of water molecules in the polyelectrolyte films, we measured the neutron reflectivity of fully hydrated and dehydrated samples. Figure 4 shows data obtained with sample B8 (64 layers organized in 8 r.u.'s; PSS and PAH deposited from 3 M NaCl) under the following conditions: (a) as prepared from H_2O solutions (same data as those shown in Figure 3a, upper trace); (b) after dehydration (3 d) over P_2O_5; (c) after rehydration of dehydrated sample in D_2O.[21] The hydrated samples were measured at ~100% r.h. of the respective water species. Common to all three reflectograms is a complicated structure that is *not* simply caused by Bragg reflections and regular Kiessig fringes. Rather, the amplitude of the Kiessig fringes varies greatly for different orders of the interference. In the vicinity of the second Bragg reflection, the Kiessig amplitude is so large that it is similar to the Bragg intensity; this generates the impression of a "split" Bragg peak. Generally, Kiessig fringes of odd order appear much smaller than fringes of even order.

The data have been analyzed in four levels of sophistication: (1) The thickness of the repeat units and the total film thickness have been estimated from the position of Bragg peaks and the spacings of the Kiessig fringes. (2) The structure was modeled as a series of strata which were characterized in terms of their thicknesses, SLDs, and interface roughness values. (3) Such models were also interpreted in terms of their molecular composition[14] (composition-space refinement) which imposes constraints on the models resulting from the physically acceptable range of parameters. (4) Further constraints were imposed on such models by *simultaneous* analysis of the related data sets (i.e., of the neutron reflectivity of the sample as prepared from H_2O-based solutions, the dehydrated and the rehydrated sample in which H_2O has been replaced with D_2O).

In the following we will discuss sequentially steps 2−4 of these evaluations, aiming at a detailed molecular picture of the structure of polyelectrolyte multilayer films.

We have not been able to describe satisfactorily the highly resolved neutron reflectivity data of sample B8 in the framework of the model used for samples of series A in which all r.u.'s were considered equivalent (identical thickness and scattering length densities of the

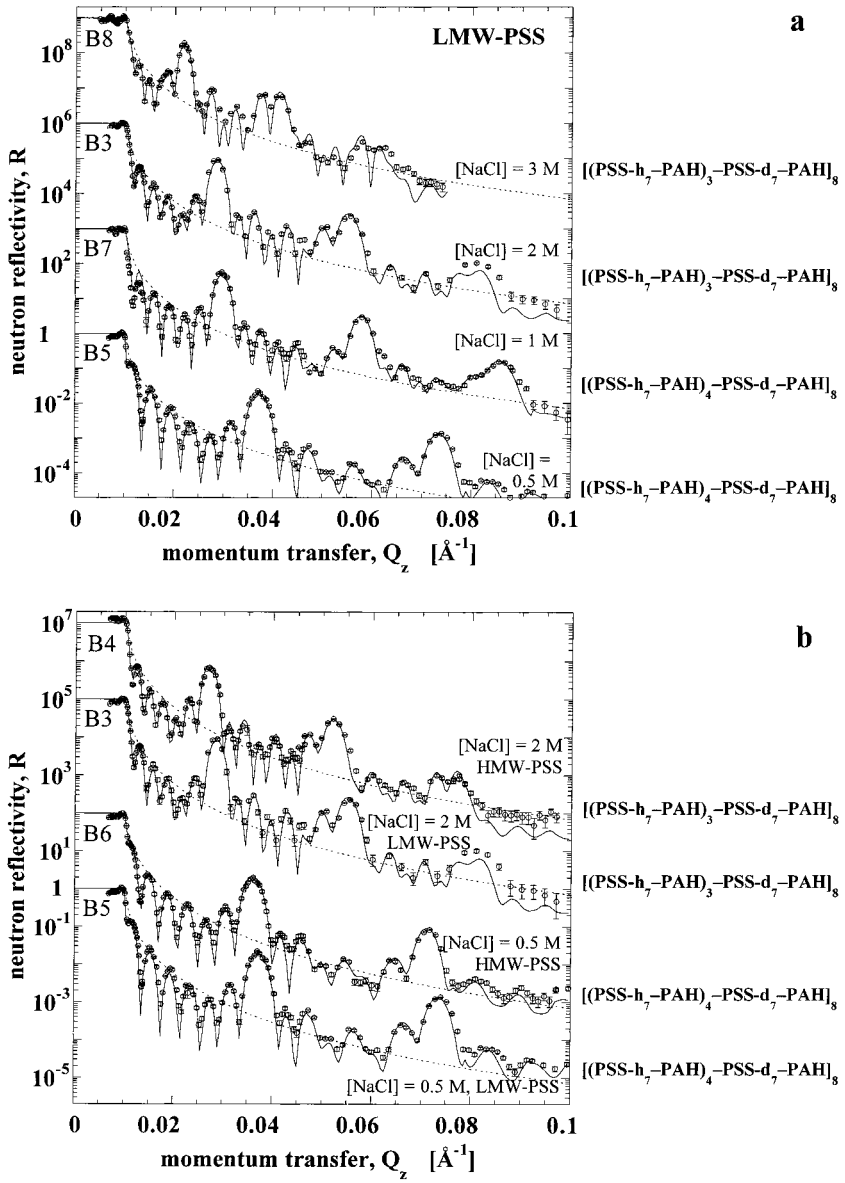

Figure 3. Comparison of neutron reflectivity data sets of polyelectrolyte multilayer samples prepared from different salt solutions (a) and using PSS of different molecular weights (b), cf. Table 1. (a) Neutron reflection from samples B8, B3, B7, and B5 (top to bottom). For clarity, data sets B8, B3, and B7 have been multiplied by 10^9, 10^6, and 10^3, respectively. (b) Neutron reflection from samples B4, B3, B6, and B5 (top to bottom). For clarity, data sets B4, B3, and B6 have been multiplied by 10^7, 10^5, and 10^2, respectively. All sample films are composed of 8 r.u.'s that contain 8 (B3, B4, B8) or 10 (B5, B6, B7) individual layers each. The data points are supplemented with continuous lines representing the best-fit models as described later in the text. The instrumental resolution has been included in the fits. Dotted lines indicate the Fresnel reflectivity of the Si substrate.

strata). In an earlier investigation of sample A2, we found from indirect arguments that the layers deposited immediately onto the solid substrate are thinner than those further away.[11] However, an assumption that the first or the first and second r.u.'s within samples of series B were of lower thickness than the remaining r.u.'s did not improve the quality of the model fits.[22] Only if it was assumed that *two particular* r.u.'s, namely the first and the fifth in the sequence of eight that form the sample film B8, are notably thinner than the remaining 6 r.u.'s, a *significantly* improved agreement between the experimental data and the reflectivity model was observed. Moreover, such a defect model reproduces with great fidelity the particular structure of the spectra, in which every other Kiessig fringe has a larger amplitude than the intervening ones.[23]

A very accurate description of the experimental datais obtained with a model in which the thicknesses of all r.u.'s within the sample are varied in the fit, whereas the SLDs of all equivalent layers are assumed to be equal. This model incorporates a relatively large number of adjustable parameters ($p = 14$ for an individual structure or $p = 18$ if three related data sets shown in Figure 4 are simultaneously evaluated using a composition-space refinement approach, see section 2b). We believe, however, that this model is well suited to describe the structure of the surface films, because (a) the adjusted thickness values show a regular pattern and (b) the same pattern is repeated in the model structures describing the data sets of the hydrated (H_2O), dehydrated, and rehydrated (D_2O) sample, *even if they are analyzed without cross-references to each other*. This pattern of the adjusted layer thickness values is shown in Figure 5a. Open symbols refer to the analysis of the individual data sets displayed in Figure 4; the filled symbols result from the composition-space

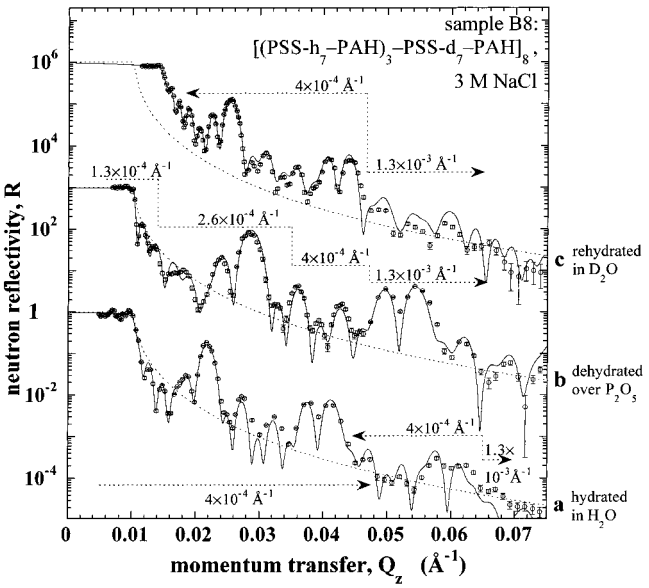

Figure 4. Neutron reflectivity of sample B8 determined at TAS8 with high resolution. (a) Sample as prepared from H_2O-based solutions; (b) after dehydration over P_2O_5 for 3 d; (c) after rehydration of the dehydrated sample in D_2O. a and c were measured at ∼100% r.h. in H_2O and D_2O, respectively. The data points are supplemented with continuous lines representing the best-fit models as described later in the text. The instrumental resolution has been included in the fit. Dotted lines indicate the Fresnel reflectivity of the Si substrate. For clarity, data sets c and b have been multiplied by 10^6 and 10^3, respectively.

refinement analysis of all three situations simultaneously. The thickness of the first r.u. is only ∼75% of the average value. The next thickness values are already larger than the average and show a monotonic increase. The fifth r.u., deposited after cleaning the reaction vessels, is reduced in its thickness to ∼90% of the average value. The last three r.u. thickness values are again above average and show a monotonic increase. As a guide for the eye, the figure includes exponential functions that were adjusted to the model parameters in a least-squares fit. They indicate how r.u.'s in the model acquire a constant thickness after starting from a small value when material is deposited on the functionalized substrate or on the polyelectrolyte surface after the cleaning of the vessels.

If the thickness of an adsorbed polyelectrolyte layer correlates with the number density of attachment sites at the interface, the observed increase of the layer thickness values with increasing number of layers is straightforward to comprehend. The number of attachment sites is particularly small for a substrate which is smooth on the atomic level and onto which a molecularly thin layer of ABS has been grafted. Typically, the first molecular polyelectrolyte layer attains only ∼50% of the thickness of a layer adsorbed far from the substrate.[11] Subsequently, the interdigitation between adjacent layers is of a molecular length scale, ∼12 Å.[11] Dangling loops and tails of a deposited polyionic layer provide an increasing number of adsorption sites for each subsequent generation of polyelectrolyte molecules as the thickness of the respective previous layers increases. Thus, layers are expected to increase in thickness from a low value at the atomically flat functionalized substrate to a limiting value. This limit is reached if either the previous layer forms a dense core that limits interpenetration by the next generation of polyions or interdigitation occurs to such an extent that it leaves less than 50% of the adsorbed polyions to form an increment layer that supports adsorption of the following layer. Upon drying the partly completed polyelectrolytic interface in the laboratory air, the polyelectrolyte may have rearranged to form such a dense core or adsorption of surface active pollutants from the air may have lead to a reduction in adsorption sites. Each of the two effects, or both simultaneously, result in the observed reduction of the thickness of the fifth r.u. as quantified in Figure 5a. According to the fit (included in the figure), the substrate-induced deviation from the equilibrium thickness decays exponentially as $\exp(-n/n_0)$, where $n_0 = 4-5$ layers (0.5−0.6 r.u.).

To exemplify the situation, Figure 5b shows a comparison of experimental data and two different reflectivity models: the "perfect lattice" (thin line) and the "fuzzy lattice" (fat line). Both models were composition-space refined (see sections 2b and 2c). Only the result for the hydrated sample is shown in the figure. It is easily appreciated that the structure of the neutron data is reproduced with high fidelity by the variable layer thickness approach. By contrast, the best-fit model using a constant layer thickness is incapable of describing the experimental data, notably in the region between the Bragg reflections. This is reflected in the χ^2 values associated with the two models, $\chi^2 = \sim 90$ (perfect lattice) and $\chi^2 = \sim 25$ (fuzzy lattice).[24] The corresponding SLD profiles (thick line, fuzzy lattice; thin line, perfect lattice) are shown in the inset. It is recognized how the positions and the peak SLD values[25] in the fuzzy lattice model vary along the $\hat{z}$ coordinate.

Although a discussion of the polyelectrolyte film structure in terms of models that are characterized by thickness and SLD values of layers ("SLD approach") is convenient, the interpenetration between polymer chain segments in adjacent layers infers a problem. We reported previously[11] that the precision in determining the thickness of a single deuterated layer within a stratified film is rather poor. This is because the apparent roughness of the interface between protonated and deuterated strata is comparable with the deuterated layer thickness. Because the two parameters are coupled, the Erf-smeared SLD profiles, and thus the model reflectivities, are similar if a thin deuterated layer with high SLD and a thick deuterated layer with low SLD are compared. It is then impossible to draw definite conclusions about the molecular structure of the surface film exclusively based on least-squares minimization. This situation is quantified by exploring χ^2 in the vicinity of its minimum in the multidimensional parameter space by varying one parameter freely while readjusting all others.[14] Figure 6a exemplifies this by showing the χ^2 values for model fits describing the neutron reflectivity of sample B3 (cf. Figure 3) at different PSS layer thickness values, d_{PSS}, subject to the condition that all other adjustable parameters are allowed to relax to a new local minimum. The dependence on d_{PSS} only is very weak: the variation of χ^2 is ≤5% upon varying d_{PSS} between 10 and 60 Å. The corresponding relative variations of selected adjustable parameters are shown in Figure 6b. Most parameters show a rather weak dependence on d_{PSS} with the notable exception of the SLD of the deuterated strata, ρ_n^{PSS-d}, which falls by ∼75% as d_{PSS} is varied between 10 and

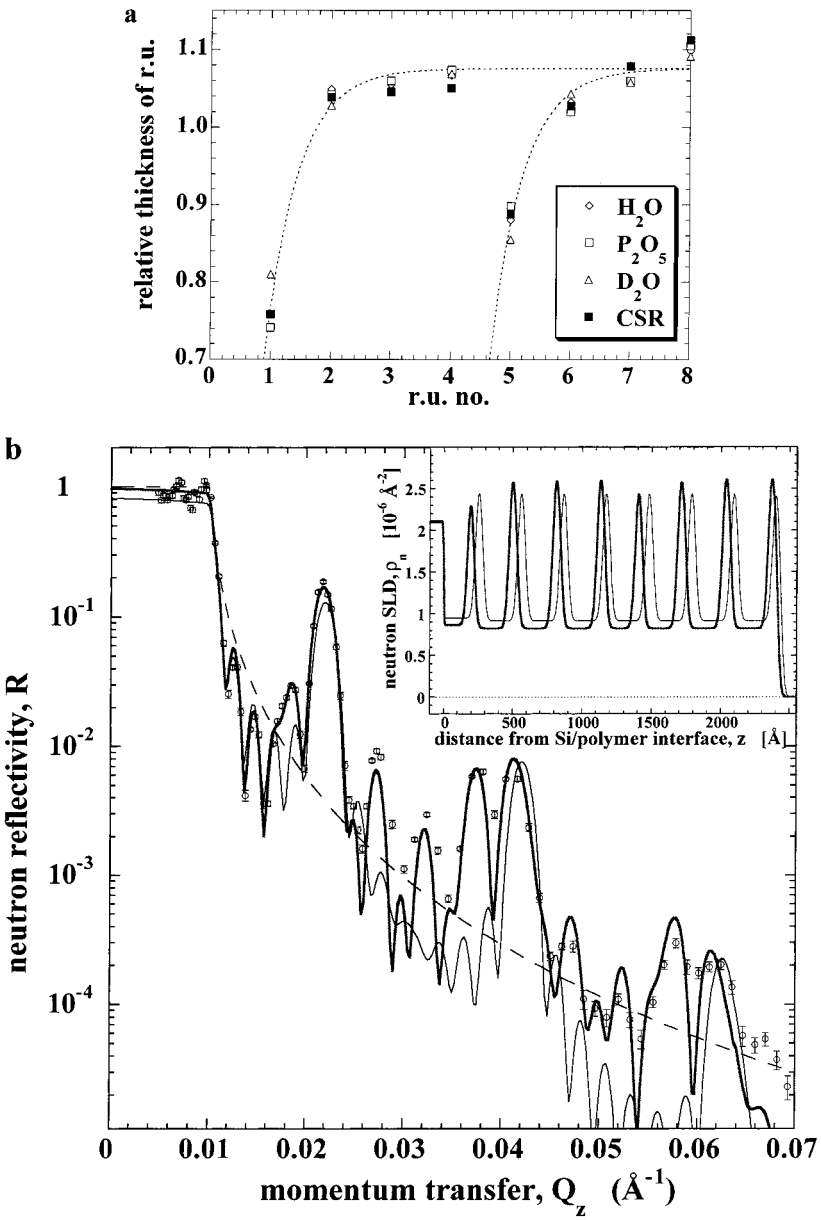

Figure 5. Details of the data modeling.(a) Variation of the relative thickness of r.u.'s within the film structure of sample B8. Open symbols show best-fit results obtained from modeling of the different data sets shown in Figure 3 without reference to each other (diamonds, sample hydrated in H_2O; squares, sample dried over P_2O_5; triangles, sample after rehydration in D_2O of the dehydrated sample). The filled symbols are best-fit results from composition-space refinement (see section 2b). The dashed lines are exponential fits to the data (see text). (b) Comparison of the best-fit models invoking a regular layer thickness (thin line) and variable layer thickness (fat line) with experimental data. Either model was refined simultaneously to all three B8 data sets (for the hydrated, dehydrated, and rehydrated samples, see section 2b). Only the data and models (as well as corresponding SLD profiles in the inset) for B8 hydrated in H_2O are shown.

60 Å. If one analyzes the actual SLD *profiles* associated with the various models differing in d_{PSS} it is evident that they are almost identical.[26] It is thus clear that the conventional layer model is insufficient for deducing a fully resolved molecular description of the sample structure. Such a description can be obtained, however, by restricting the space accessible to d_{PSS} through a molecular interpretation of the model's SLDs.[14,27]

2b. Composition-Space Approach to Model Refinement: In using a specific microscopic model in the composition-space evaluation of the data shown in Figure 3, our basic assumption was that the polyelectrolytes form molecular layers (which may or may not interpenetrate one another), as suggested by the observed Bragg reflections. Each individual layer is thought to consist of one polymeric species only. Nevertheless, because of the intermixing of chain segments of polyanions and polycations at the interface between neighboring layers, different polymer species may occur close to each other in space. It is assumed, however, that the density profile of a particular polymeric species is well described by error functions, cf. eq 1, in which σ_i may be large (even larger than one layer thickness).

Each layer consists of polymer chains, associated water, and inorganic salt that may have coadsorbed from solution. Within a polyanionic layer, the volume is filled with matter in which each styrenesulfonate monomer within the polymer chain is associated with n_w^{PSS} water molecules and n_s^{PSS} Na^+ ions. Conversely, in the polycationic layers, each allylamine monomer is associated with n_w^{PAH} water molecules and n_s^{PAH} Cl^-

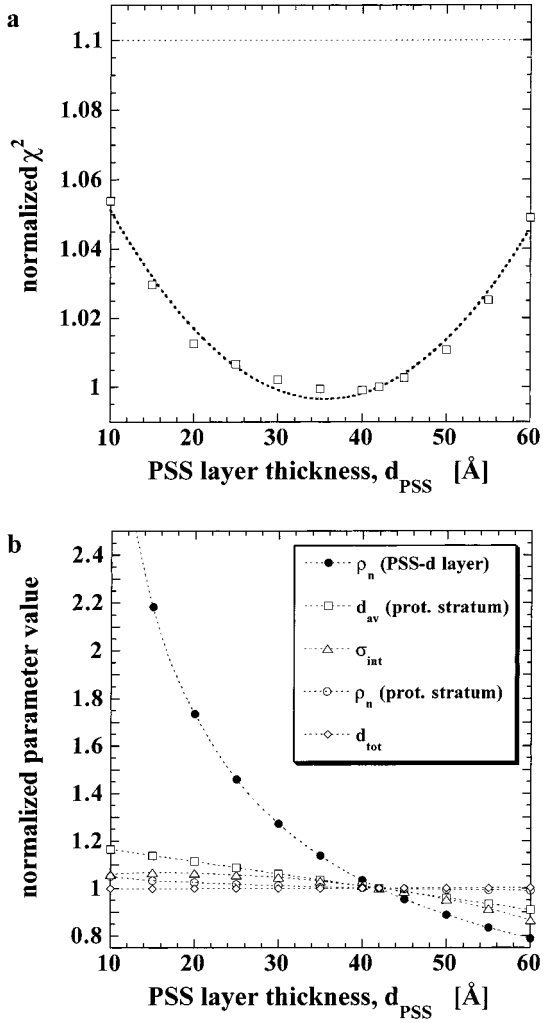

Figure 6. Model refinement of the neutron reflectivity of sample B3. (a) Sensitivity of the fit to variations of the thickness of the (deuterated) PSS layers, d_{PSS}. The dotted line is a parabolic fit to the best-fit χ^2 values at different assumed d_{PSS}. The thin dotted line at $\chi^2 = 1.1$ visualizes the criterion used to estimate the uncertainties in the composition-space refinement discussed below (cf., Figure 8). (b) Corresponding variation of selected parameters as indicated.

ions. Specifically, a volume element occupied by a polyanion chain

$$V_{pa} = V_{PSS} + n_w^{PSS} V_{water} + n_s^{PSS} V_{Na^+} \qquad (2a)$$

where V_{PSS} is the molecular volume of a styrenesulfonate monomer within the polymeric chain and the subscript "water" denotes either H_2O or D_2O. V_{pa} contains the scattering length

$$b_{pa}^{prot} = b_{PSS-h_7} + n_w^{PSS} b_{water} + n_s^{PSS} b_{Na^+} \qquad (2b)$$

or

$$b_{pa}^{deut} = b_{PSS-d_7} + n_w^{PSS} b_{water} + n_s^{PSS} b_{Na^+} \qquad (2b')$$

which leads to the local SLD

$$\rho_{pa}^{prot(deut)} = b_{pa}^{prot(deut)}/V_{pa} \qquad (2c/2c')$$

In the set of eqs 2, V_{PSS}, n_w^{PSS}, and n_s^{PSS} are unknown. Similarly, a microscopic volume associated with a polycationic chain

$$V_{pc} = V_{PAH} + n_w^{PAH} V_{water} + n_s^{PAH} V_{Cl^-} \qquad (3a)$$

holds a scattering length

$$b_{pc} = b_{PAH} + n_w^{PAH} b_{water} + n_s^{PAH} b_{Cl^-} \qquad (3b)$$

which gives an SLD

$$\rho_{pc} = \frac{b_{pc}}{V_{pc}} \qquad (3c)$$

In eqs 3, V_{PAH}, n_w^{PAH}, and n_s^{PAH} are unknown. Within the appropriate layers, V_{pc} and V_{pa} are distributed over the areas $A_{pa} = V_{pa}/d_{pa}$ and $A_{pc} = V_{pc}/d_{pc}$, respectively. Because the films are macroscopically electroneutral, A_{pa} and A_{pc} depend on each other, and thus either d_{pc} or d_{pa} is a dependent quantity. Specifically, because we expect that the salt concentration in the deposited films is small, we have assumed that $n_s^{PAH} = n_s^{PSS}$ which implies $A_{pa} = A_{pc}$ and thus $d_{pa} = d_{pc} \times V_{pa}/V_{pc}$.

The different experimental situations (neutron reflection from the sample as prepared from H_2O, after dehydration over P_2O_5, and after rehydration in D_2O, cf. Figure 4) are accounted for by specifying the isotopic identity of the water molecules in eqs 2 and 3. Upon dehydration of the pristine sample over P_2O_5, it was assumed that *all* water molecules are eliminated from the film. The packing voids that might be left within the structure are not accounted for by an increase in the polymer volumes but by a void volume factor χ relating to the original number of water molecules contained in the film:

$$V_{pa}^{dehydr} = V_{PSS} + n_w^{PSS} \chi_w^{dehydr} V_{water} + n_s^{PSS} V_{Na^+} \qquad (4a)$$

$$V_{pc}^{dehydr} = V_{PAH} + n_w^{PAH} \chi_w^{dehydr} V_{water} + n_s^{PAH} V_{Cl^-} \qquad (5a)$$

Of course, no water molecules contribute to the SLD of the strata in this state of the sample:

$$b_{pa}^{dehydr,prot(deut)} = b_{PSS-h_7(-d_7)} + n_s^{PSS} b_{Na^+} \qquad (4b/4b')$$

$$b_{pc}^{dehydr} = b_{PAH} + n_s^{PAH} b_{Cl^\pm} \qquad (5b)$$

The sample in the *re*hydrated state need not include the same number of water molecules as the pristine sample. In fact, upon modeling the data with the "SLD approach" we found that the total film thickness of the sample after rehydration was ~2.5% smaller than that of the sample as prepared from polyelectrolyte solutions in H_2O. If one assumes that no polymer molecules and no inorganic salt is removed from the film upon dehydration, then a reduction factor η is a proper correction:

$$V_{pa}^{rehydr} = V_{PSS} + n_w^{PSS} \eta_w^{rehydr} V_{water} + n_s^{PSS} V_{Na^+} \qquad (6a)$$

$$V_{pc}^{rehydr} = V_{PAH} + n_w^{PAH} \eta_w^{rehydr} V_{water} + n_s^{PAH} V_{Cl^-} \qquad (7a)$$

Note that water *does* contribute to the SLD of the volume elements here. Moreover, an exchange of deuterium (D) for H has to be accounted for on the hydrogen

positions of the PAH amine group.

$$b_{pa}^{rehydr} = b_{PSS-h_7(-d_7)} + \eta_w^{rehydr} n_w^{PSS} b_{D_2O} + n_s^{PSS} b_{Na^+} \quad (6b/6b')$$

$$b_{pc}^{rehydr} = b_{PAD} + \eta_w^{rehydr} n_w^{PAH} b_{D_2O} + n_s^{PAH} b_{Cl^-} \quad (7b)$$

In this approach, we have to determine from the fit two more unknown parameters, χ and η, whereas b_{PAD}, just as the other scattering lengths, may be calculated from tabulated values of the scattering lengths of the constituent atoms. We gain the ability to model all three measurements at different contrasts *simultaneously*, which greatly constrains the results and leads to a self-consistent molecular conception of the sample within the stated assumptions.[28]

2c. Film Structure as Revealed from Composition-Space Refinement: The composition-space refinement approach to data interpretation was applied to the neutron reflectivity data sets observed with sample B8, cf. Figure 4. Models with and without salt incorporated in the polyelectrolyte films were analyzed, yielding the following results:

(a) Assuming that *no* NaCl is included in the polyelectrolyte films (an assumption motivated by results from XPS and radiotracer techniques), we were not able to describe the neutron reflectivity results as well as with models that included salt. We found that the χ^2 of any "salt-free" model was ~6% larger than that of models with NaCl (see below).

(b) On assuming that inorganic counterions *were* included in the film, we observed distinct χ^2 minima at $d_{PSS} = 58$ Å in the refinement of the model. To reduce the number of free parameters fitted in the model, we made the following assumptions: (i) The number of polyanionic monomers equals the number of polycationic monomers in the film and $n_s^{PAH} = n_s^{PSS}$, i.e., the film is macroscopically electroneutral. (ii) H_2O or D_2O molecules within the film occupy the same volume as in bulk water. (iii) The volume of counterions within the film is the same as that of the respective ions in a NaCl crystal. (iv) Void volume within hydrated polyelectrolyte films as well as differences between the specific partial volumes of water and counterions in the films and in bulk is thus fully accounted for by the (fitted) volume of the polymers, V_{PSS} and V_{PAH}. We determined the partial volumes of the polymers in the film by adjusting only one parameter, V_{PSS}, whereas V_{PAH} was adjusted in a fixed relation to V_{PSS}. To estimate the relationship between V_{PSS} and V_{PAH}, we analyzed energy-minimized computer models of oligomers ($n = 1 \ldots 6$) of the respective polyelectrolytes and determined the Connolly surfaces[29] measured with various probe radii r.[30] The volume increment per monomer was determined by linear regression with respect to n. We found van der Waals volumes per monomer (probe radius used in the determination of the Connolly surface, $r = 0$) of $V_{PSS}^{VdW} \sim 131$ Å^3 and $V_{PAH}^{VdW} \sim 50$ Å^3, leading to $V_{PAH}/V_{PSS} \equiv \varphi \sim 0.382$. To analyze the situation that PAH and PSS are packed in films, probe radii $r > 0$ were used. One may expect that the volume of the bulkier PSS grows more rapidly than that of PAH as r increases. This was indeed observed, see Figure 7. For $r < 5$ Å, V_{PSS} increases almost linearly (Figure 7a), and φ decreases linearly for $r \geq 1.5$ Å (Figure 7b). A crossover to $\varphi = $ const. is observed as $r \to 0$. We used $\varphi = 0.33$, corresponding to $r \sim 3.5$ Å, to retrieve the structural model discussed below. This value is consistent with the result, retrieved a posteriori from the model fit, that assigns a volume $V_{PSS} \sim 200$ Å^3, cf. Figure 7a.

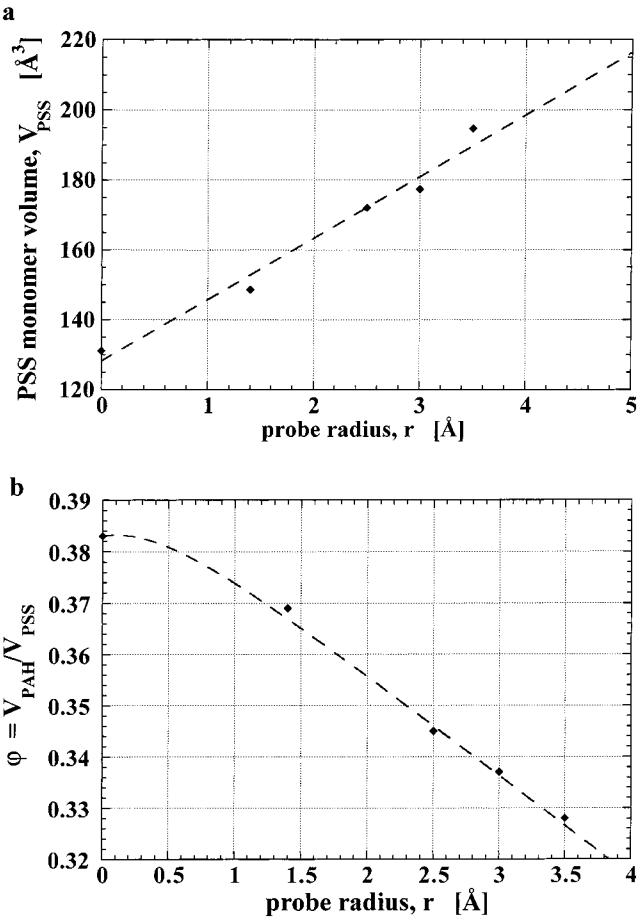

Figure 7. Estimate of the polyelectrolyte monomer volumes from molecular models. (a) PSS volume as obtained from the slope of oligomer volumes, V_{PSS}^n, vs degree of polymerization, n ($n = 1 \ldots 6$). The molecular models were energy-minimized in vacuo, followed by a short (100 ps) molecular dynamics run before measuring their Connolly surfaces with various probe radii, r. (b) The same procedure has been applied to PAH and the ratio V_{PAH}/V_{PSS} determined. Dashed lines are guides for the eye.

Table 3 gives the numerical values of the relevant constants used in the model describing the experimental results shown in Figure 4 and summarizes the results derived from the fit. The salt content, n_s, is poorly determined in the fit because the model is rather insensitive to it. To estimate confidence limits of the determined model parameters listed in Table 3, we have accepted changes in χ^2 of 10% above its global minimum value. The quality of the fit as a function of d_{PSS} is shown in Figure 8, which allows direct comparison with Figure 6a (SLD modeling approach). This comparison shows clearly the capability of the composition-space refinement approach (note the different scale of the ordinates in Figures 6a and 8 and bear in mind that both figures relate to samples deposited from solutions with different ionic strengths). Figure 8 includes data points, indicated by solid diamonds, that show χ^2 values obtained from the "salt-free" model ($n_s = 0$). It is apparent that their χ^2 is well below the chosen uncertainty limit of $\Delta\chi^2 = 0.1$. Hence one cannot decide from neutron reflectivity data whether inorganic salt is included within the deposited polymer film.

Table 3. Structure of Sample B8 as Obtained from Simultaneous Composition-Space Refinement of the Neutron Reflectivities of the Hydrated (H_2O), Dehydrated (P_2O_5), and Rehydrated (D_2O) Film

quantity	symbol	value	uncertainty	status
H_2O volume	V_{H_2O}	29.9 Å^3	−	constant
D_2O volume	V_{D_2O}	30.25 Å^3	−	constant
Na^+ volume	V_{Na^+}	6.3 Å^3	−	constant
Cl^- volume	V_{Cl^-}	38.55 Å^3	−	constant
total film thickness (H_2O)[a]	$d_{tot}(H_2O)$	2427 Å	± 7 Å	dependent quantity
PSS layer thickness (H_2O)[b]	d_{PSS}	58.0 Å	± 7 Å	variable
PAH layer thickness (H_2O)[b]	d_{PAH}	17.7 Å	± 5 Å	dependent quantity
PSS monomer volume	V_{PSS}	201 Å^3	± 2 Å^3	variable
PAH monomer volume	V_{PAH}	67 Å^3	± 1 Å^3	dependent quantity
H_2O per PSS monomer[c]	n_w^{PSS}	6.0	± 1.3	variable
H_2O per PAH monomer[c]	n_w^{PAH}	1.0	± 1.5	variable
water void volume factor[d]	χ_w^{dehydr}	0.415	± 0.002	variable
rehydration factor[e]	η_w^{rehydr}	0.925	± 0.003	variable
Na^+/Cl^- per monomer	$n_s^{PAH} = n_s^{PSS}$	0.5	± 0.5	variable
substrate roughness	σ_{Si}	5 Å	−	constant
interface roughness[f] (H_2O)[a,g]	$\sigma_{int}(H_2O)$	28.3 Å	± 1.3 Å	variable
interface roughness[f] (P_2O_5)[a,g]	$\sigma_{int}(P_2O_5)$	23.2 Å	± 0.4 Å	variable
interface roughness[f] (D_2O)[a,g]	$\sigma_{int}(D_2O)$	32.5 Å	± 0.5 Å	variable
total film thickness (P_2O_5)[a]	$d_{tot}(P_2O_5)$	1834 Å	± 6 Å	dependent quantity
total film thickness (D_2O)[a]	$d_{tot}(D_2O)$	2363 Å	± 7 Å	dependent quantity

[a] Determined for hydrated (H_2O), dehydrated (P_2O_5), and rehydrated (D_2O) film. [b] Quoted results are average numbers. They have to be multiplied by 0.759 (first r.u.), 1.039 (second r.u.), 1.046 (third r.u.), 1.051 (4th r.u.), 0.888 (5th r.u.), 1.028 (6th r.u.), 1.078 (7th r.u.), and 1.112 (8th r.u.) to obtain the actual structure. [c] In fully hydrated film as prepared from H_2O-based solutions. [d] On dehydration, each water molecule leaves $\chi_w^{dehydr} \times V_{H_2O}$ of void volume within the polymer film. [e] After rehydration of the fully dehydrated film with D_2O, for each original H_2O molecule, η_w^{rehydr} D_2O molecules are recovered into the polymer network. [f] Between adjacent polymer strata within the film. [g] The model is virtually insensitive to the film/air roughness $\sigma_{f/a}$, which has formally been included with constant values ($\sigma_{f/a}$ (H_2O/D_2O) = 24 Å, $\sigma_{f/a}$ (P_2O_5) = 20 Å) in the fit.

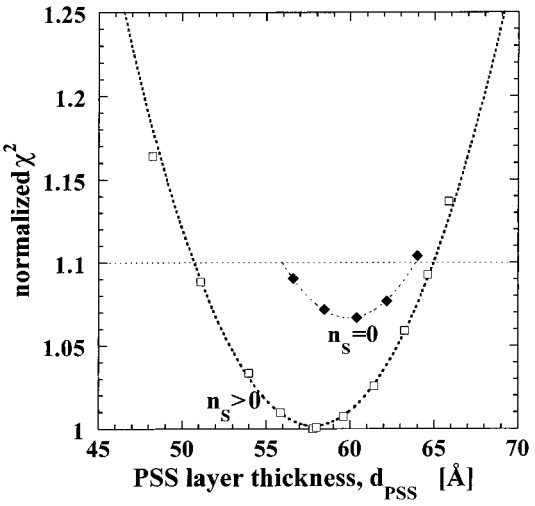

Figure 8. χ^2 from composition-space refinement of the data from sample B8 (hydrated, dehydrated, and rehydrated) as a function of the PSS layer thickness, d_{PSS}.

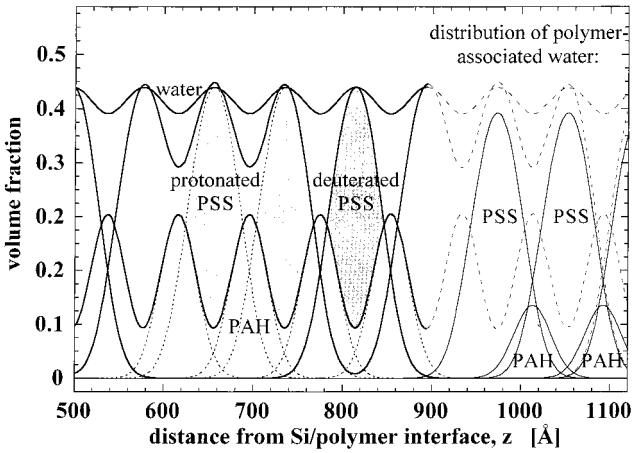

Figure 9. Detailed structure of the stratified film (sample B8 as prepared from H_2O) in terms of volume fraction of the constituents along the surface normal, $\hat{z}$. In this presentation, n_s = 0.4 has been assumed, such that the sum of volume fractions of PSS, PAH, and water is less than 100% (~ 95% throughout the film). Above z = 900 Å, the distribution of water associated with the different polyelectrolyte species is indicated.

Some of the results of the composition-space refinement of the data from sample B8 are visualized in Figure 9. Shown are the volume fractions of PSS and PAH and of water, and on the right-hand side of the plot, the volume fraction of water associated with either of the two polyelectrolyte species is indicated.

2d. Structure as a Function of Ionic Strength: Figure 10 summarizes the results of reflectivity measurements from samples prepared from deposition solutions with various ionic strengths (Figure 3a). It is apparent that the layer pair thickness d_{lp} is proportional to the ionic strength, I. The internal roughness between adjacent layers as prepared from H_2O-based solutions scales with the layer thickness ($\sigma_{int} \sim 0.4 \times d_{lp}$). It was shown above that structural details as revealed from neutron reflectometry do not depend strongly on the assumption of whether salt is incorporated into the film. Hence we conclude that the ratio d_{PAH}/d_{PSS} is fairly independent of I, which justifies writing d_{PSS} and d_{PAH} as *constant* fractions of d_{lp}. Thus, $d_{PSS} \equiv 0.76 \times d_{lp}$ and $d_{PAH} \equiv 0.24 \times d_{lp}$, as indicated in the figure.

2e. Structure as a Function of the Degree of Polymerization: An evaluation of the data presented in Figure 3b, where films deposited from polyelectrolyte solutions of various molecular weights M_w have been investigated, reveals that the effect of M_w on the structure is rather small. This is appreciated qualitatively by simply comparing the upper and lower pairs of neutron reflectivity data sets shown in the figure. A quantitative evaluation shows that an increase of the degree of polymerization from P_w = 900 to P_w = 5000

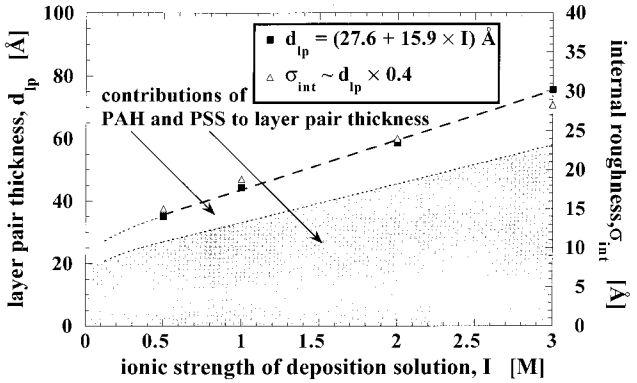

Figure 10. Structure of polyelectrolyte films as deposited from solutions with various ionic strengths, *I*. The scales on the ordinate are chosen such that the correspondence between the layer pair thickness, d_{lp} (filled squares, left scale), and the interfacial roughness between adjacent polymer layers, σ_{int} (open triangles, right scale), becomes apparent. The equation and the heavy dashed line represent a linear fit to the data. Based on the situation revealed by analyzing sample B8 in a composition-space refinement, d_{lp} is broken down into individual layer thickness values. The light dotted lines and the grayed areas indicate these contributions of the individual layers to the layer pair thicknesses. For $I \rightarrow 0$ a nonlinear reduction of the layer thickness is indicated, as discussed in the text.

for the PSS leads to an increase in the thickness of the r.u.'s of ≤3% (films deposited from 0.5 M NaCl) and of ≤6% (2 M NaCl). If one assumes that structural relations as measured with sample B8 apply and that the PAH layer thicknesses are equal in all samples, it may be estimated that the increase in PSS layer thickness is less than 4.5% (0.5 M NaCl) and less than 10% (2 M NaCl). It may be concluded that the adsorption process is strongly cooperative. A quantitative evaluation of the cooperativity, however, will require more data at different P_w values.

Discussion

The formation of layered supramolecular architectures has made major inroads into materials science.[31] The sequential deposition of alternately charged polyelectrolytes in molecularly thin films is a fundamental process in this field, because it sets the stage for the immobilization of such diverse colloidal particles as proteins or clay minerals and may result in the development of novel electroluminescent devices.[7,12,32] We have systematically studied the formation of molecular films from simple polyelectrolytes and have harnessed the full power of neutron reflectometry for a detailed characterization of their structure.

The following statements about the structure of a polyelectrolyte multilayer film deposited from 3 M salt solutions of PAH and PSS may be made without addressing the issue of salt incorporation into the polyions:

(1) The film structure is stratified, as discussed above, despite the fact that the interdigitation between polymer trains from adjacent layers is of the same order as the total layer thickness. In addition, the relative thickness variation of the strata, as discussed earlier, is verified in the composition-space refinement of the data (see Figure 5a). This is reflected in the SLD profiles shown in the inset in Figure 5b as a pronounced modulation of the ρ_n peak heights of the deuterated layers, where the first peak (at $z = 195$ Å) and the fifth peak (at $z =$ 1405 Å) are significantly lower than the others. The relative thickness values may be determined with an accuracy of ±3%, and are independent of the assumed salt content of the film. We have thus resolved the internal structure of the polyelectrolyte multilayer film with high resolution.

(2) The hydration of the both polyions is quite different on the basis of H_2O molecules per residue in the film. Whereas ∼6 H_2O are associated with each PSS monomer, only 1 H_2O is attached to each PAH monomer. If, however, the *volume fractions* of H_2O and the respective polyions are compared (Figure 9), the result is much closer; only twice as much H_2O volume is associated with PSS as with PAH.

The distribution of PSS and PAH organized in layers interpenetrating along the $\hat{z}$ direction is shown in Figure 9 on the left-hand side, below $z = 900$ Å. Individual layer profiles are indicated by dotted lines, whereas profile envelopes are rendered as solid black lines. Note that due to the interpenetration, the volume fraction of PSS is *larger* in the center of the PAH layer than the volume fraction of PAH itself. As recognized at $z = 815$ Å, even in the center of a *deuterated* PSS layer, the tails of the *protonated* PSS layers join to form a fraction of ∼0.5% of the total volume. The total water concentration is roughly constant at ∼42% volume fraction throughout the film. At the right-hand side, above $z = 900$ Å, the volume fraction of polymer-associated water (solid lines) is given with respect to the polymer itself (dashed lines).

(3) Dehydration over P_2O_5 leads to shrinkage of the film. This is expected as water evaporates from the structure. Neutron reflection measurements, however, reveal the particulars in great detail. (a) Water molecules that are removed from the polymer network leave a void volume within the film. On average, ∼40% of the liberated water volume is *not* filled by the polymer upon film shrinkage, presumably because of steric hindrance inferred in the polymer chains. The shrinkage of the film occurs congruently and homogeneously. A reduction of the interface roughness between adjacent layers is observed upon dehydration which is proportional to the shrinkage of the film along the surface normal, i.e., the polymer network tightens on dehydration without rearrangement of the loop structures within the layers. As far as one can judge from the neutron reflectivity measurements, no lateral inhomogeneity is inferred by the dehydration process. It is not revealed whether one of the polyelectrolyte species holds on to water more tightly than the other, but in any case the thickness ratio of the adjacent layers shifts by a few percent upon dehydration because of the larger volume fraction contained in the PSS chains.

(4) Upon rehydration (in this case with D_2O), the film structure swells. The recovery of water into the polymer network is almost, but not quite, complete with respect to the film structure as prepared from H_2O. Roughly 95% of the desiccated water molecules return into the film structure. This slight decrement could be caused by an isotopic effect or by rearrangements in the polymer structure. The observation that the interface roughness between adjacent layers within the structure is slightly *larger* after rehydration whereas the overall film thickness is slightly *smaller* points to the latter interpretation.

In Figure 10 we have compiled the results from modeling neutron reflection measurements on samples deposited from solutions with various ionic strengths *I*.

In doing so, we extrapolated the detailed structural conception of the sample deposited from 3 M salt concentration on the other experimental situations. A quantitative comparison with earlier work,[3] in which the thickness increments of PAH−PSS multilayer structures were measured using X-ray reflectometry is not straightforward, because PAH layers were deposited from salt-free solutions in the earlier preparations. The PAH layers in those preparations are thus presumably thinner than those in the work presented here. Moreover, those samples were characterized at various stages during the preparation (after the deposition of 6, 8, 10, 15 ... layer pairs), and in the light of the results obtained in the current investigation one has to assume that layers deposited after the inspection of the surfaces with X-rays are significantly thinner than those obtained in a continuous process (cf. section 2a and Figure 5a). Finally, radiation damage of polymer molecules exposed to X-rays during a reflection experiment cannot be neglected, such that layer thickness results are systematically low if determined with X-rays. All these caveats do not apply to the current work. Thus, Figure 10 represents the structure of PAH−PSS multilayer films determined with the least-impact characterization technique available to date for the investigation of layered supramolecular architectures. Although the general conclusion[1,3] that the self-assembly of polyanion/polycation films may be fine-tuned by variation of the ionic strength of the deposition solution still holds, one has to add that details of the structure may sensitively depend on environmental parameters.

Although both the layer pair thickness and the internal layer roughness values scale fairly linearly between ionic strengths $I = 0.5$ and 3 M NaCl in the preparations solution, a linear extrapolation to $I = 0$ cannot be made. Experimentally it has been observed that layer pairs of PAH and PSS deposited at $I = 0$ are much thinner, $d_{lp} = 8$ Å (cf. Figure 14a in ref 1), than the value $d_{lp} \sim 27.5$ Å expected from a linear extrapolation of the neutron results to $I = 0$. Theoretically, the dependence of the Debye screening length $1/\kappa$ for small ionic strengths I is

$$\frac{1}{\kappa} \sim I^{-1/2}$$

Therefore, an increase of the layer (or layer pair) thickness with increasing I is expected to be nonlinear at low I and may also follow a square-root dependence. Such a dependence is indicated tentatively in the low-I regime of Figure 10, and a square-root dependence is indeed approximately observed in X-ray reflection experiments on similar systems (B. Lehr and G. Decher, unpublished results).

The most fundamental result of this work is the observation that polyelectrolyte multilayer films grow in a nonlinear fashion close to the substrate. We have argued that this occurs due to a roughening of the polymer/polymer interfaces upon deposition of successive polyanion/polycation layer pairs which leads to a progressively larger number of binding sites for polyelectrolyte chains adsorbing from solutions. The situation equilibrates quickly, after the deposition of 4−5 molecular layers. This equilibration occurs because the microscopic structure of adsorbed polyelectrolyte layers adjacent to aqueous solutions is obviously so flaccid, presenting multiple trains and loops to the aqueous adphase, that adsorbing polycounterions interpenetrate deeply into the deposited film. From the model that describes the experimental data best we infer occasional close contacts between polymer molecules whose centers of gravity are located 4 molecular layers apart (cf. Figure 9). The coincidence of this number with the equilibration length scale strongly suggests a causal relationship between the layer thickness equilibration and the interpenetration between the molecular species. Further away from the substrate than ∼8 molecular layers, the layer thickness is constant within the experimental error *if the environmental parameters are kept fixed during the dipping process*. The occasional partial dehydration of the surfaces between dipping events, and potentially other preparation flaws, may lead to unexpected results.

In earlier work,[11] we precisely determined the internal (protonated polymer/deuterated polymer) and the external (polymer/air) interfacial roughness values from a comparison of neutron and X-ray reflectivity data. We concluded then that the internal roughness is significantly larger than the external roughness and attributed the difference to chain-chain interdigitation between adjacent polymer layers. In this work we have observed the same trend, namely smaller values of $\sigma_{f/a}$ than of σ_{int}, although the external roughness of the polymer film toward the air cannot be precisely determined from the neutron reflectivity data without cross-reference to X-ray data.

In contrast, recent X-ray/neutron reflectivity measurements on PAH/PSS multilayer systems incorporating deuterated poly(phenylenevinylene), PPV-d, as a functional component in molecular polymer interface films, have led to the conclusion that $\sigma_{int} \leq \sigma_{f/a}$ in those systems.[12] This may be understood from the preparation process of the PPV layers, which includes deposition of a sulfonated precursor polycation and its subsequent conversion into the conjugated polymer by heating under vacuum. The product is immiscible with PSS, located in adjacent layers, so that phase separation between the two compounds is likely to occur upon curing of the polymer film. As a result, the interface between the deuterated and the protonated layers is expected to be sharper than those between the other nondeuterated polycations and polyanions (PPV-d was the *only* deuterated substance used in the multilayer structure reported on in ref 12). With the help of the results presented here, another apparent inconsistency in the conclusions of Tarabia et al.[12] may be resolved. In their discussion, Tarabia et al.[12] are puzzled by the fact that according to their X-ray measurements, the mass density of the PAH/PSS spacer layers appears to be 1.34 g/cm^3, whereas from the neutron data a mass density of 0.79 g/cm^3 has been deduced. They attribute this tentatively to the incorporation of Ca^{2+} ions into the multilayer structure, which might increase the X-ray SLD above the value expected from the neutron SLD of the polyelectrolyte layers. Apparently, however, a huge Ca^{2+} concentration would be required to achieve consistency among the two models. In light of our work it seems that Tarabia et al. in their interpretation have simply failed to account for water included in the hydrophilic films during the measurements. A numerical conversion of our results for the neutron SLD used to describe a PSS-h_7/PAH double layer *hydrated with H_2O* into an equivalent electron density yields $\rho_e = 0.42$ e$^-$/Å^3, close to the value $\rho_e = 0.43$ e$^-$/Å^3 reported by

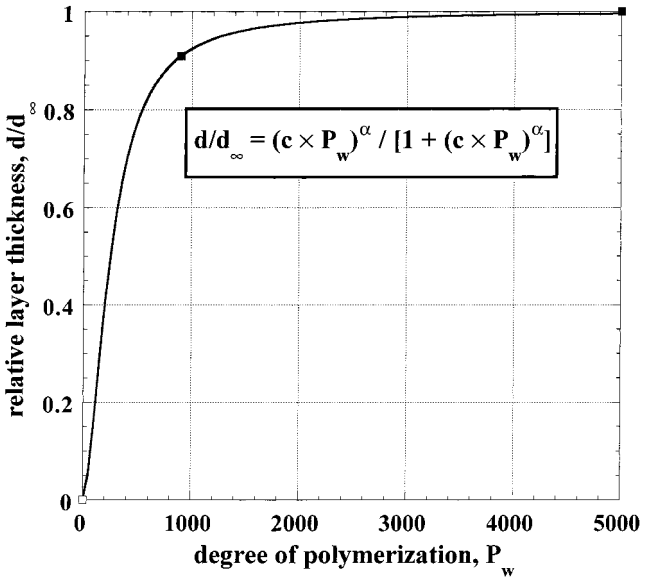

Figure 11. Dependence of the PSS layer thickness on the degree of polymerization of the polyanion. The line is a guide for the eye suggesting cooperativity of the adsorption process.

Tarabia et al. At the same time, the neutron SLD of the layer pair reported here is $\rho_n = 0.8 \times 10^{-6}$ Å^{-2}, which is also consistent with the refractive index reported in ref 12 for the spacer layers in various samples ($\sim 0.9 \times 10^{-6}$ Å^{-2}), *without assuming counterion* (Ca^{2+}) *inclusion into the layer structure*. Although Tarabia et al.[12] do not report on the humidity control of the sample environment during their measurements, it seems natural to suppose that H_2O is included within the polyelectrolyte layers in their samples, and that the H_2O content in their samples is similar to or slightly less than the one found in this work. To enable further comparison of ref 12 and the present work, we note that the SLDs found in the present work translate to average polyelectrolyte mass densities of ~0.81 and ~1.13 g/cm^3, based on a PAH/PSS double layer in the fully hydrated and the fully dehydrated samples, respectively. For comparison, the hypothetical mass density expected for efficiently packed polyelectrolyte films, i.e., the sum of the monomer masses devided by the sum of their volumes as obtained from this study (cf. Table 3), would amount to ~1.51 g/cm^3. Obviously, this poses an upper limit for the value that the mass density can possibly attain.

Figure 11 displays the weak dependence of the PSS layer thickness of self-assembled polymer multilayer films on the degree of polymerization, P_w. Clearly, more measurements have to be performed before definitive conclusions can be drawn. It is obvious from the two experimental results with $P_w \sim 900$ and 5000, however, that the adsorption to charged surfaces is a strongly cooperative process. To stress this, an empirical function

$$\frac{d}{d_\infty} = \frac{(\text{const.} \times P_w)^\alpha}{1 + (\text{const.} \times P_w)^\alpha} \qquad (8)$$

is included in Figure 11 as a visual guide. It remains to be seen whether the adsorption of polyelectrolytes to charged interfaces of the kind used in this work can be described in terms of the cooperativity models generally used to describe binding processes of biological macromolecules.[33]

Conclusions

Using neutron reflectometry, we have resolved the internal structure of self-assembled polyelectrolyte multilayer films to high resolution and have developed a detailed molecular picture of such systems by analyzing the data with a composition-space refinement technique. We have shown that such surface films consist of stratified structures in which polyanions and polycations within individual layers intimately interdigitate one another. Nevertheless, the deposition technique leads to results that are very predictable if well-defined and constant environmental conditions are maintained during the preparation. For the PSS/PAH couple adsorbed onto atomically flat surfaces, a roughening of successively deposited layers leads to a progressively larger number of adsorption sites for consecutive generations of adsorbed polymer, and thus to an increase in layer thicknesses with an increasing number of deposited layers. Because of the interdigitation between adjacent polyelectrolyte species, however, this increase settles quickly into an equilibrium thickness. In fully hydrated films (100% r.h.), water occupies ≥40% of the volume within the films. About twice as much water (by volume) is associated with PSS as with PAH. Incorporated inorganic salt plays only a minor role, if any. The equilibrium thickness of the deposited layer structure may be fine-tuned via the ionic strength of the solutions used for the preparation. A quantitative comparison with earlier work by Decher and Schmitt[3] supports their general conclusion but yields film thicknesses that are a factor of ~2 larger. Possible reasons for this discrepancy were discussed above. In contrast to the ionic strength of the deposition solutions, the degree of polymerization of the polyanions used in the preparation plays only a minor role in determining the overall structure of the deposited films.

Acknowledgment. We are grateful for neutron beam time at Risø National Laboratory and for funding by the EC-TMR program. Thanks are due to K. Lehmann, Leipzig, for his assistance with some of the measurements. This work was also supported by the DFG (Sonderforschungsbereich 294, Teilprojekt C9), the BMBF (contract no. 03-LO4LEI-8), and the Fonds der Chemischen Industrie (to M.L. and G.D.).

References and Notes

(1) Decher, G. In *Comprehensive Supramolecular Chemistry*; Sauvage, J. P.; Hosseini, M. W., Ed.; Pergamon Press: Oxford, 1996; Vol. 9; p 507.
(2) Decher, G.; Hong, J.-D.; Schmitt, J. *Thin Solid Films* **1992**, *210/211*, 831.
(3) Decher, G.; Schmitt, J. *Prog. Colloid Polym. Sci.* **1992**, *89*, 160.
(4) Cheung, J. H.; Fou, A. F.; Rubner, M. F. *Thin Solid Films* **1994**, *244*, 985.
(5) Ferreira, M.; Rubner, M. F. *Macromolecules* **1995**, *28*, 7107.
(6) Fou, A. C.; Rubner, M. F. *Macromolecules* **1995**, *28*, 7115.
(7) Gao, M.; Richter, B.; Kirstein, S. *Adv. Mater.* **1997**, *9*, 802.
(8) Hong, J. D.; Lowack, K.; Schmitt, J.; Decher, G. *Prog. Colloid Polym. Sci.* **1993**, *93*, 98.
(9) Hammond, P. T.; Whitesides, G. M. *Macromolecules* **1995**, *28*, 7569.
(10) Diederich, A.; Lösche, M. *Adv. Biophys.* **1997**, *34*, 205.
(11) Schmitt, J.; Grünewald, T.; Decher, G.; Pershan, P. S.; Kjaer, K.; Lösche, M. *Macromolecules* **1993**, *26*, 7058.
(12) Tarabia, M.; Hong, H.; Davidov, D.; Kirstein, S.; Steitz, R.; Neumann, R.; Avny, Y. *J. Appl. Phys.* **1998**, *83*, 725.
(13) Vaknin, D.; Kjaer, K.; Als-Nielsen, J.; Lösche, M. *Makromol. Chem., Macromol. Symp.* **1991**, *46*, 383.

(14) Vaknin, D.; Kjaer, K.; Als-Nielsen, J.; Lösche, M. *Biophys. J.* **1991**, *59*, 1325.
(15) Bouwman, W. G.; Vigild, M.; Findeisen, E.; Kjaer, K.; Feidenhans'l, R.; Mol, E. A. L. *J. Neutr. Res.* **1997**, *5*, 133.
(16) Bouwman, W. G.; Pedersen, J. S. *J. Appl. Crystallogr.* **1996**, *29*, 152.
(17) Als-Nielsen, J.; Kjaer, K. In *Phase Transitions in Soft Condensed Matter*; Riste, T.; Sherrington, D., Ed.; Plenum Press: New York, 1989; p 113.
(18) Similarly, the ABS layers directly on the Si substrates cannot be discriminated from the first (protonated) PSS layers and have thus not been explicitly accounted for in the models described in detail later.
(19) From the peak positions, $Q_z = 2\pi/d_{r.u.}$ we may preliminarily deduce the thickness of the repeat unit, $d_{r.u.} = 105$ Å (A1), respectively 157 Å (A2), consistent with a common layer pair thickness of 52 Å. From this, in turn, we deduce for A3 the expected position of the first Bragg peak to be $Q_z = 2\pi/(52$ Å$) \sim 0.12$ Å^{-1}. No indication of a Bragg peak was detected in the Q_z range around 0.12 Å^{-1} (data not shown). On the other hand, the expected spacing of the Kiessig fringes, $\Delta Q_z = 2\pi/(10 \times 52$ Å$) \sim 0.012$ Å^{-1}, is in agreement with experimental observations.
(20) HMW (samples B4 and B6): degree of polymerization $P_w = 5000$ for PSS; LMW (samples B3 and B5): $P_w = 900$; PAH (in all samples): $P_w = 530-700$.
(21) Instrumental resolution ΔQ_z: (a) 4×10^{-4} Å^{-1}, $Q_z < 0.064$ Å^{-1}; 1.3×10^{-3} Å^{-1}, above. (b) 1.3×10^{-4} Å^{-1}, $Q_z < 0.014$ Å^{-1}; 2.6×10^{-4} Å^{-1}, 0.014 Å$^{-1} < Q_z < 0.035$ Å^{-1}; 4×10^{-4} Å^{-1}, 0.035 Å$^{-1} < Q_z < 0.047$ Å^{-1}; 1.3×10^{-3} Å^{-1}, above. (c) 4×10^{-4} Å^{-1}, $Q_z < 0.046$ Å^{-1}; 1.3×10^{-3} Å^{-1}, above.
(22) To explain the unusual structure of the reflectograms shown in Figures 3 and 4, we also tested several defect models to find out whether a particular type of defect increases the quality of the model fit significantly. These tests included models in which the structures were laterally inhomogeneous, i.e., it was assumed that two slightly different r.u.'s lead to incoherent summation of different reflectivities. In other attempts it was assumed that the r.u.'s had one particular thickness near to the substrate and a different one further away, after the deposition of k layers, or that the thickness of one particular r.u., at a position k', was different from that of all other r.u.'s. Although all these defect structures afforded slightly better fits than the original model in which all r.u.'s were assumed equivalent, these improvements were only due to the higher number of adjustable parameters which all defect models necessarily infer.
(23) At the same time we became aware of a flaw in the sample preparation procedure: We cleaned the vessels containing the dipping solutions at half-time of the film fabrication process to avoid deterioration of the layer quality by contaminations transfected between the vessels in the course of dipping cycles. During the time used for cleanup and mixing of new polyelectrolyte solutions, the half-completed samples were exposed to ambient air, and it must be assumed that the surface of the fourth r.u. was affected either by structural reorganization or by adsorption of contaminations from the laboratory air.[26]
(24) χ^2 is computed by taking only statistical errors of the neutron counts into account. Due to the marked structure in the spectra exceedingly small systematic errors in Q_z lead to a significant increase of the measured χ^2.
(25) SLD peak values vary slightly at the center positions of the deuterated layers in different r.u.'s because their thickness, d_{deut}, varies with $d_{r.u.}$, whereas σ_{int} has been assumed identical at all internal interfaces. Because 2 σ_{int} is of the order of d_{deut}, the SLD never reaches the "bulk value" of a deuterated PSS layer.
(26) Schmitt, J. Ph.D. Thesis, Mainz University, 1996.
(27) Lösche, M. Habilitation Thesis, Mainz University, 1994.
(28) To reduce the complexity of the model, we have also used a composition-space refinement approach with averaged neutron SLD of the protonated layers, similar to the procedure used with samples A1−A3. We observed, however, that this approximation leads to molecular models slightly different from that obtained with the more detailed description.
(29) Connolly, M. L. *Appl. Crystallogr.* **1983**, *16*, 548.
(30) We used Cerius^2 (Molecular Simulations, Inc., Cambridge, U.K.) with a van der Waals scale factor of 1.0.
(31) Knoll, W. *Curr. Opin. Colloid Interface Sci.* **1996**, *1*, 137.
(32) Hong, H.; Davidov, D.; Avany, Y.; Chayet, H.; Faraggi, E. Z.; Neumann, R. *Adv. Mater.* **1995**, *7*, 846.
(33) Cantor, C. R.; Schimmel, P. R. *Biophysical Chemistry. Part III: The Behavior of Biological Macromolecules*; W. H. Freeman: New York, 1980.

MA980910P